Chinese Chemical Letters 31 (2020) 836–840

Contents lists available at ScienceDirect

Chinese Chemical Letters

journal homepage: www.elsevier.com/locate/cclet

Communication

Platinum monolayers stabilized on dealloyed AuCu core-shell nanoparticles for improved activity and stability on methanol oxidation reaction

Weihua Guo, Xiaozhang Yao, Lingyi Peng, Bingqing Lin, Yongqiang Kang, Lin Gan*

Division of Energy and Environment, Graduate School at Shenzhen, Tsinghua University, Shenzhen 518055, China

ARTICLE INFO

Article history:
Received 8 May 2019
Received in revised form 4 June 2019
Accepted 10 June 2019
Available online 11 June 2019

Keywords:
Platinum monolayers
Methanol oxidation reaction
Core-Shell nanoparticles
Dealloying
Stability

ABSTRACT

Deposition of platinum (Pt) monolayers (Pt_{ML}) on Au substrate represents a robust strategy to maximally utilize the Pt atoms and meanwhile achieve high catalytic activity towards methanol oxidation reaction for direct methanol fuel cells owing to a substrate-induced tensile strain effect. However, recent studies showed that Pt_{ML} on Au substrate are far from perfect smooth monoatomic layer, but actually exhibited three-dimensional nanoclusters. Moreover, the Pt_{ML} suffered from severe structural instability and thus activity degradation during long-term electrocatalysis. To regulate the growth of Pt_{ML} on Au surface and also to improve its structural stability, we exploit dealloyed AuCu core-shell nanoparticles as a new substrate for depositing Pt_{ML}. By using high-resolution scanning transmission electron microscopy and energy dispersive X-ray elemental mapping combined with electrochemical characterizations, we reveal that the dealloyed AuCu core-shell nanoparticles can effectively promote the deposition of Pt_{ML} closer to a smooth monolayer structure, thus leading to a higher utilization efficiency of Pt and higher intrinsic activity towards methanol oxidation compared to those on pure Au nanoparticles. Moreover, the Pt_{ML} deposited on the AuCu core-shell NPs showed substantially enhanced stability compared to those on pure Au NPs during long-term electrocatalysis over several hours, during which segregation of Cu to the Au/Pt interface was revealed and suggested to play an important role in stabilizing the Pt_{ML} catalysts.

Direct methanol fuel cells (DMFC) represent one of the most promising clean energy sources for portable consumable electronics due to their high energy densities. However, the sluggish anodic methanol oxidation reaction (MOR) has greatly limited the efficiency and power density of DMFCs and generally requires the use of large amounts of noble metal electrocatalysts like platinum (Pt) [1–4]. In addition, Pt also suffers from severe poisoning effect by the CO intermediate ($-CO_{ads}$) formed during MOR [3]. To decrease the usage and increase the activity of Pt, Brankovic *et al.* developed an efficient catalyst design strategy by deposition of a monoatomic-thick Pt layer (namely, Pt monolayer, hereafter denoted as Pt_{ML}) on a second substrate through surface-limited redox replacement of a pre-formed underpotential deposited Cu monolayer [5–9]. These Pt_{ML} could ideally achieve 100% Pt utilization, thus showing promising mass-normalized catalytic activities [10–13]. Deposition on different substrates can also result in strain/ligand effect on the Pt_{ML} in combination of the can sensitively modulate the Pt surface catalytic activities [7,14,15]. In particular, a tensile strain on the Pt_{ML} was achieved on Au substrate due to a larger lattice parameter (or atomic radius) of Au compared to Pt, leading to enhanced adsorption of hydroxyl ($-OH$) from water [12]. The enhanced OH formation could promote the oxidation of $-CO_{ads}$ or a direct oxidation of $-COH_{ads}$ to CO_2 without the formation of CO_{ads}, thus leading to enhanced MOR activities.

While the monolayer structure of Pt_{ML} was generally assumed and has been observed on Pd substrate [16], recent studies show that Pt_{ML} grown on Au substrate, either bulk [17,18] or nanoparticle (NP) surfaces [18,19], is far from a perfect monolayer film but exhibits three-dimensional (3D) rough agglomerates (namely, a Volmer-Weber growth mode), which not only reduces the utilization of Pt atoms but also weakens the tensile strain effect. This is probably due to the large lattice parameter difference (4%) between Au (4.08 Å) and Pt (3.92 Å), while lattice mismatch between Pd (3.89 Å) and Pt (3.92 Å) is on 0.77% [20,21]. Indeed, conformal overgrowth of Pd on Pt nanocube seeds into epitaxial core-shell structure have been demonstrated, whereas overgrowth of Au on the Pt seed resulted in anisotropic heterostructure [20]. In addition to the effect of lattice parameter, the weak interaction

* Corresponding author.
E-mail address: lgan@sz.tsinghua.edu.cn (L. Gan).

https://doi.org/10.1016/j.cclet.2019.06.018
1001-8417/

between Au and Pt (or more favorable Pt-Pt interactions) [17] and much lower surface energy of Au compared to Pt [22,23] were also considered to contribute to the formation of 3D Pt agglomerates on Au. Moreover, the 3D Pt agglomerates on Au surface were unstable during long-term operation particularly under high potentials, leading to substantial catalyst degradation [19,24]. To promote the formation of a smooth Pt monolayer on Au {111} surface, a CO stabilization strategy was developed by utilizing a stronger interaction of CO with Pt compared to that with Au [17]. However, once removing the CO adsorbent, three-dimensional Pt agglomerate re-generate, suggesting a great limitation of the CO stabilization strategy.

In this paper, we exploit a new approach to regulate the growth of smooth Pt_{ML} catalysts on Au surface by utilizing dealloyed Cu-Au core-shell NPs as the substrate. The use of dealloyed Cu-Au NPs not only reduce the usage of noble metal Au, but also can efficiently promote the growth of Pt_{ML} on the Au surface closer to a smooth monolayer, leading to improved MOR activity. This was confirmed by using high resolution scanning transmission electron microscopy (STEM), energy dispersive X-ray (EDX) spectroscopic mapping and electrochemical characterizations. The core-shell compositional fine structures of the as-grown Pt_{ML} on dealloyed Au-Cu core-shell NPs before and after long-term MOR electrocatalysis were further carefully characterized, suggesting substantially improved stability after long-term MOR electrocatalysis in comparison with those grown on pure Au NPs. This study provides a new way to stabilize smooth Pt monolayers on Au surface for enhanced electrocatalytic properties on MOR.

The AuCu NPs were prepared by a previously-reported seeded solvothermal method using pre-synthesized Au NPs as the seed [25] and then supported on a high surface area carbon (Vulcan XC) (detailed experimental procedures are presented in the supplementary material). Fig. 1a shows TEM image of the supported AuCu NPs, which exhibit a uniform particle size with an average diameter of 4.5 nm (particle size distribution analysis in Fig. S1 in Supporting information) and a composition close to $Cu_{50}Au_{50}$ as confirmed by EDX analysis. For comparison, a home-made pure Au catalyst with the average particle size of 5.1 nm supported on Vulcan XC was also prepared (the TEM image is shown in Fig. S1). Dealloyed AuCu core-shell NPs (denoted as D-AuCu) were then prepared by electrochemical cycling (200 cycles) of the AuCu NPs in 0.1 mol/L $HClO_4$ between 0.05 V and 1.2 V (Unless otherwise specified throughout the paper, all potentials are normalized to reversible hydrogen electrode, RHE) at 500 mV/s (Fig. 1b). During this process, surface non-noble Cu atoms were gradually removed as indicated by the large oxidative peaks at around 0.58 V. A smaller reductive peak at around 0.55 V can be also observed and can be ascribed to underpotential deposition (UPD) of part of leached Cu^{2+} on the Au surface. However, this reductive peak was much smaller than the oxidative peak related to Cu leaching, meaning that the UPD rate is far lower than that of Cu leaching. After 200 cycles, no oxidative/reductive peak can be observed, indicating the complete removal of surface Cu. The AuCu alloy core and Au shell in the dealloyed Au-Cu NPs are confirmed by EDX mapping (Fig. 1c) as well as the Z-contrast STEM image (Fig. S2 in Supporting information), and the average composition was determined to be $Au_{75}Cu_{25}$ from large area EDX analysis. Fig. 1d presents the X-ray diffraction (XRD) patterns of the pristine AuCu, the D-AuCu and the pure Au catalyst, all of which show a face-centered-cubic structure. The AuCu alloy NPs manifest an obvious shift of diffraction peaks to higher angles relative to pure Au NPs, indicating a decreased lattice parameter (3.96 Å) compared to Au (4.08 Å) due to Cu alloying. After leaching the surface Cu, the average lattice parameter of the D-AuCu NPs (4.04 Å) increases but still range between the pure Au (4.08 Å) and pure Pt (3.92 Å). In another word, the dealloyed AuCu NPs can still result in a tensile strain for subsequently deposited Pt_{ML}.

The dealloyed Au-Cu NPs were then applied as the substrate for depositing Pt_{ML} by the well-established redox replacement of UPD Cu_{ML} process. Firstly, a Cu_{ML} was underpotentially deposited on the dealloyed Au-Cu core-shell NPs in N_2-satruated $CuSO_4$ and H_2SO_4 solution and then subsequently replaced by K_2PtCl_4 in N_2-saturated 50 mmol/L H_2SO_4. Following previous reports, the use of Pt^{2+} precursor in H_2SO_4 solution enables one-by-one replacement of Cu by Pt^{2+} [9,18]. The as-deposited catalyst was denoted as D-AuCu@Pt. The pristine AuCu NPs were not directly used as the substrate for Pt_{ML} since not only the outmost-surface Cu but also the near-surface Cu atoms would be replaced by Pt^{2+} precursor, leading to a AuPt alloy surface instead of a Pt monolayer on top of Au substrate. For comparison, Pt_{ML} was also deposited on the pure Au NPs following the same protocol (denoted as Au@Pt). Fig. 2 presents the high-angle annular dark field (HAADF) STEM characterization of the D-AuCu@Pt catalyst and the Au@Pt catalyst. Consistent with our previous findings [19], the Au@Pt catalyst (Fig. 2a, and more images in Fig. S3 in Supporting information) exhibits an irregularly shape with a high surface roughness and sharp corners/protrusions, significantly different from the near spherical shape of original Au NPs (Fig. S1). High resolution STEM (HR-STEM) image (Fig. 2b) also presents a non-uniform image contrast across the NP as indicated by the intensity line profile shown in the inset, indicating a non-uniform Pt deposition on the surface. EDX mapping in Fig. 2c also evidences a non-uniform deposition of Pt, with the sharp corners identified as the formation of 3D Pt nanoclusters. In contrast, the D-AuCu@Pt catalyst demonstrates similarly smooth NP surface as the original D-AuCu NPs (Fig. 2d). No prominent islands or sharp corners are observed on the surface of D-AuCu@Pt particles and the HR-STEM image (Fig. 2e) exhibits a uniform image contrast across the whole NP, indicating successful deposition of smooth Pt_{ML}. This was corroborated by EDX-mapping (Fig. 2f), where Pt distributes more homogeneously on the D-AuCu NPs without apparent Pt-rich sharp corners.

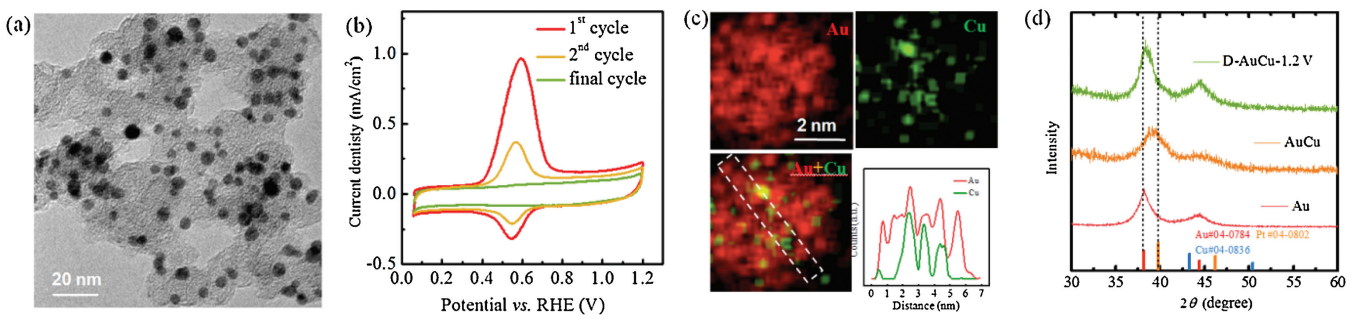

Fig. 1. (a) TEM image of the as-prepared AuCu NPs supported on Vulcan XC carbon support. (b) CV curves (the 1st, 2nd and last cycle) of electrochemical dealloying of AuCu NPs by 200 cycles between 0.05 V and 1.2 V at 500 mV/s in N_2-saturated $HClO_4$ solution. (c) EDX mapping and line profile of D-AuCu NPs, evidencing a AuCu alloy and an Au shell. (d) XRD patterns of pristine AuCu NPs, D-AuCu NPs, and pure Au NPs.

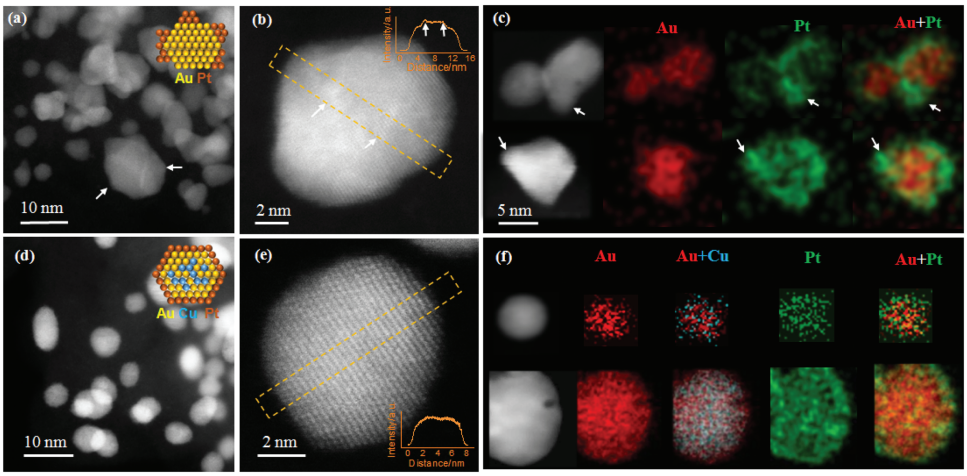

Fig. 2. HAADF-STEM images, EDX-mapping and structural model of D-AuCu@Pt (a–c) and Au@Pt (d–f) nanoparticles.

The more uniform deposition of Pt_{ML} on the D-AuCu core-shell NPs compared to those on pure Au NPs indicates a significant role of Cu at the core in regulating the growth of smooth Pt_{ML} on the Au surface. Geometrically, alloying of Cu at the core can induce decreased lattice parameter of Au and thus reduced lattice mismatch between Au and Pt, which benefits a continuous epitaxial growth of Pt_{ML} instead of Volmer-Webber growth. Thermodynamically, the 3D agglomerate structure of Pt on pure Au surface was previously ascribed to much lower surface energy of Au compared to Pt, which drives the segregation of Au over Pt [17,26]. On dealloyed Au-Cu core-shell NPs, the compressive strain exerted by the AuCu alloy core would in principle increase the surface energy of the Au shell compared to unstrained pure Au surface, since the latter represents the most stable state and thus has the lowest surface energy. Thus, decreased surface energy difference between Au and Pt is expected and favors the formation of 2D Pt_{ML} on D-AuCu NPs

The surface composition of the D-AuCu@Pt and Au@Pt catalyst can be further evaluated by surface adsorption/desorption during cyclic voltammetry (CV) in N_2-saturated 0.1 mol/L $HClO_4$ solution (Fig. 3a). A clear hydrogen adsorption/desorption feature on Pt can be clearly observed between 0.05 V and 0.35 V. In addition, there are two reduction peaks at 0.4–0.9 V and 0.9–1.4 V corresponding to the reduction of Pt surface oxides and Au surface oxides formed under high potentials, respectively [27]. From the charge associated with the hydrogen adsorption/desorption on Pt (210 $\mu C/cm^2$) and Au oxide reduction (180 $\mu C/cm^2$ for a upper potential limit of 1.5 V) [28], the surface compositions of the Au@Pt and the D-AuCu@Pt catalyst were estimated to be 47% Pt and 75% Pt, respectively. The higher Pt surface composition on the D-AuCu@Pt catalyst is in good accordance with its higher Pt coverage as revealed by STEM-EDX mapping.

CO stripping was also performed to gain further insight into the catalyst surface adsorption properties (Fig. 3b). The onset and peak potentials of the CO stripping are highly sensitive to the binding energy of Pt with CO and with hydroxyl from water, both of which are critical for oxidation of adsorbed CO on Pt surface [12]. Adsorption of CO on Au can be ruled out since no CO stripping peak can be observed on pure Au NPs (Fig. S4 in Supporting information), consistent with previous findings [27]. The commercial Pt/C (Johnson Matthey 3000, 2 nm) shows the most delayed CO oxidation among the three catalysts, since CO adsorbs strongly yet hydroxyl adsorbs too weakly on pure Pt surface for CO oxidation. Due to a stronger adsorption of OH on Pt surface with a tensile strain, an earlier CO stripping was observed on both Au@Pt and D-AuCu@Pt catalysts compared to pure Pt catalyst. On par with Au@Pt, the onset potential of CO stripping on the D-AuCu@Pt catalyst is further lower, indicating a further enhanced adsorption of hydroxyl. MOR electrocatalytic activity measurement (Fig. 3c) show that the D-AuCu@Pt catalyst produced 3-fold enhancement in terms of mass-normalized activity at 0.8 V. When normalized to the ECSA of Pt, the D-AuCu@Pt catalyst also demonstrates substantially enhanced (1.5×) surface-specific activities than that of the Au@Pt catalyst and much higher (4.5×) compared to commercial Pt catalyst (Fig. 3d). This result indicates that, although the lattice parameter of the dealloyed Cu-Au NPs decreased compared to Au NPs, Pt_{ML} deposited on D-AuCu NPs may experience even higher tensile strain than those on Au NPs. This is reasonable since the 3D nanocluster morphology of Pt_{ML} on the

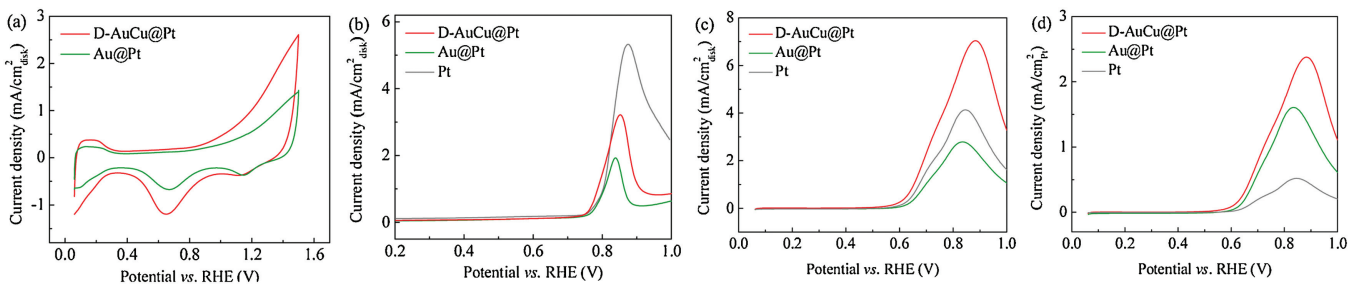

Fig. 3. Electrochemical characterization and methanol oxidation activities of D-AuCu@Pt and Au@Pt catalyst in comparison with a commercial Pt/C (Johnson Matthey 3000, 2 nm) electrocatalyst. (a) CVs in N_2-saturated 0.1 mol/L $HClO_4$ solution at 100 mV/s. (b) CO stripping in 0.1 mol/L $HClO_4$ at 10 mV/s. (c) MOR polarization curves recorded in N_2-satruated 0.5 mol/L CH_3OH +0.1 mol/L $HClO_4$ at a scanning rate of 10 mV/s. (d) MOR polarization curves normalized to the ECSA of different catalysts. Catalyst loadings on the electrode for the D-AuCu@Pt and the Au@Pt catalyst were controlled to be 16 $\mu g_{Au}/cm^2$, while catalyst loading for Pt/C catalyst was 16 $\mu g_{Pt}/cm^2$.

latter would greatly compromise the substrate-induced tensile strain effect.

Electrocatalytic stability of the D-AuCu@Pt catalyst on the MOR was further evaluated by long-term chronoampemetry holding at 0.6 V for 12 h, in comparison with the Au@Pt catalyst measured at identical conditions (Fig. 4a). Both the two catalysts exhibit obvious activity drop, which can be ascribed to the accumulation of CO_{ad} intermediate which poisons the Pt surface. In particular, the Au@Pt catalyst almost show no activity after 8 h. The D-AuCu@Pt catalyst, although degrades first as well, maintains a stable electrocatalytic activity after 10 h, thus showing improved stability than the Au@Pt catalyst. To gain atomic origin of the different stability, we further conducted STEM-EDX mapping of the aged catalyst NPs. The aged D-AuCu@Pt NPs (Fig. 4c) generally still show a high coverage of the Pt_{ML} shells, despite lower than those before stability test. In contrast, the aged Au@Pt NPs show much lower Pt coverage on the surface or even no Pt at all (Fig. 4d). To quantitatively analysis the Pt coverage, the perimeter of the Pt_{ML} on the surface was measured and divided by the perimeter of the projected image of Au NPs, as illustrated in Fig. S5 (Supporting information). The statistical results are shown in Fig. 4b. The Pt coverages of all the analyzed Au@Pt NPs (mostly below 40%) are much lower than those of the D-AuCu@Pt catalyst (above 60%). These results suggest an obvious structural change of the Pt_{ML} on Au NPs during extended electrocatalytic stability test, which would exacerbate the activity degradation due to both decreased ECSA and weakened tensile strain effect. Subsurface Cu alloying can effectively suppress the structural instability of Pt_{ML}, thus contributing to enhanced electrocatalytic stability.

Besides the structural stability of Pt_{ML}, it appears that the distribution of Cu in the D-AuCu@Pt catalyst substantially changed after the stability test. In contrast to the pristine D-AuCu NPs where Cu is mainly confined at the core, the EDX mappings in Fig. 4c show that part of Cu migrates to the interface between Au and Pt_{ML}. This can be quantitatively revealed by the line profiles along the dash line regions of particle c1 and particle c3, as shown in Figs. 4e and f, respectively. The detailed reason of Cu interface segregation was unclear at present but could be induced by alleviated interface strain energy. Similar interface segregation phenomenon has been observed in random grain boundaries of Ni-Bi bulk alloys [29] and twin boundaries of Mg bulk alloys containing impurities like Zn and Gd [30], yet the segregation at the nanoscale interfaces of core-shell NPs has not been reported and needs further studies. It is however highly speculated that Cu segregated at the Au/Pt interfaces may play an important role in stabilizing the Pt_{ML} on Au due to the much stronger Cu-Pt and Cu-Au interaction compared to Pt-Au.

In conclusion, we demonstrate an efficient approach to stabilize Pt monolayers on Au surface by using dealloyed AuCu core-shell NPs as substrate. The existence of Cu at the NP core not only decreased the usage of the precious metal Au but also reduced the lattice mismatch and surface energy difference between Au and Pt, thus favoring the epitaxial growth of a smooth Pt_{ML} on the Au-rich shell. As a result, the D-AuCu@Pt catalyst shows a higher ECSA of Pt and enhanced mass activity compared to the Au@Pt catalyst. Moreover, the obtained smooth Pt_{ML} on the D-AuCu NPs also showed higher specific catalytic activity than the Au@Pt catalyst due to a higher strain effect. During long-term steady state

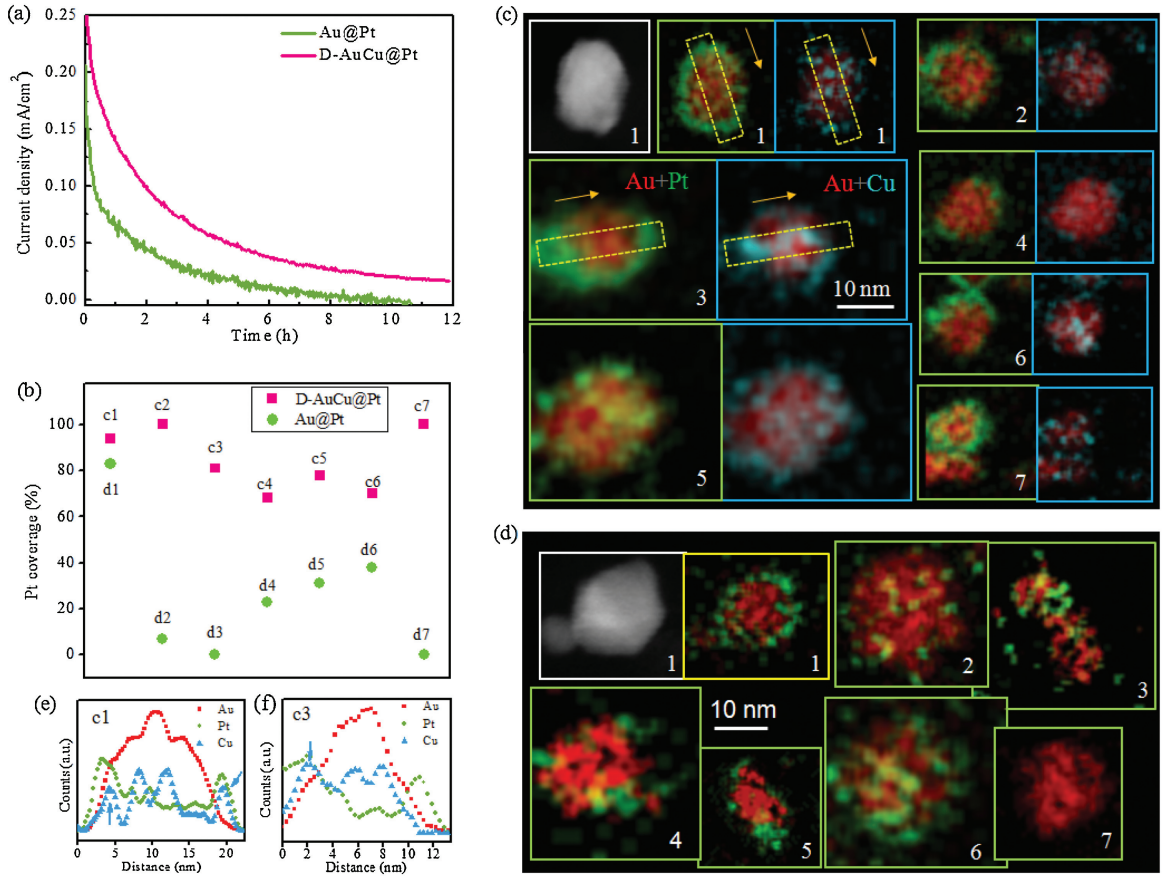

Fig. 4. Electrocatalytic stability and structural changes of the D-AuCu@Pt and the Au@Pt catalyst. (a) Long-term stability test by holding at 0.6 V for 12 h. (b) Statistical analysis of the Pt coverage in different D-AuCu NPs (particles c1-c7 in (c)) and the Au NPs (particle d1-d7 in (d)) after stability test based on the EDX mapping shown in (c) and (d), respectively (c and d) EDX elemental mapping of the D-AuCu@Pt and Au@Pt catalyst after the stability test. (e and f) EDX line profiles along the directions as shown in the elemental mapping of particle 1 and 3 in (c), respectively.

electrocatalytic stability test by holding at 0.6 V for 12 h, the D-AuCu@Pt catalyst largely maintained a high Pt coverage (above 60%) and achieved a stable electrocatalytic activity, while the Au@Pt catalyst showed significantly decreased Pt coverage and pronounced activity degradation (completely inactive after 10 h). In addition, EDX mapping suggests that Cu segregated at the interface between Au and Pt after the long-term stability test, which may play an important role in stabilizing the Pt_{ML} due to strong Cu-Pt and Cu-Au interaction. The utilization of dealloyed core-shell NPs as the substrate provide a new strategy for fine-tuning the growth of atomically smooth Pt_{ML} electrocatalysts on noble metal substrates as well as their electrocatalytic activity and stability.

Acknowledgments

We thank the financial supports by National Natural Science Foundation of China (NSFC, Nos. 21573123 and 51622103), the Local Innovative and Research Teams Project of Guangdong Pearl River Talents Program (No. 2017BT01N111), Guangdong Natural Science Foundation for Distinguished Young Scholars (No. 2016A030306035), and Basic Research Program of Shenzhen (No. JCYJ20160531194754308) in China. This work made use of the TEM facilities at the Electron Microscopy Laboratory, Materials and Devices Testing Center, Graduate School at Shenzhen, Tsinghua University.

Appendix A. Supplementary data

Supplementary material related to this article can be found, in the online version, at doi:https://doi.org/10.1016/j.cclet.2019.06.018.

References

[1] X. Zhao, M. Yin, L. Ma, et al., Synth. Lect. Energy Environ. Technol. Sci. Soc. 4 (2011) 2736.
[2] J.N. Tiwari, R.N. Tiwari, G. Singh, K.S. Kim, Nano Energy 2 (2013) 553–578.
[3] B. Braunchweig, D. Hibbitts, M. Neurock, A. Wieckowski, Catal. Today 202 (2013) 197–209.
[4] L. Gan, H. Du, B. Li, F. Kang, J. Power Sources 191 (2009) 233–239.
[5] S.R. Brankovic, J.X. Wang, R.R. Adzic, Surf. Sci. 474 (2001) L173–L179.
[6] J. Zhang, Y. Mo, M.B. Vukmirovic, et al., J. Phys. Chem. B 108 (2004) 10955–10964.
[7] R.R. Adzic, J. Zhang, K. Sasaki, et al., Top. Catal. 46 (2007) 249–262.
[8] S.E. Bae, D. Gokcen, P. Liu, et al., Electrocatalysis US 3 (2012) 203–210.
[9] D. Gokcen, Q.Y. Yuan, S.R. Brankovic, J. Electrochem. Soc. 161 (2014) D3051–D3056.
[10] K. Sasaki, H. Naohara, Y. Cai, et al., Angew. Chem. Int. Ed. 49 (2010) 8602–8607.
[11] M. Shao, K. Shoemaker, A. Peles, et al., J. Am. Chem. Soc. 132 (2010) 9253–9255.
[12] M. Li, P. Liu, R.R. Adzic, J. Phys. Chem. Lett. 3 (2012) 3480–3485.
[13] S. Khateeb, S. Guerreo, D. Su, et al., J. Electrochem. Soc. 163 (2016) F708–F713.
[14] J.L. Zhang, M.B. Vukmirovic, Y. Xu, et al., Angew. Chem. Int. Ed. 44 (2005) 2132–2135.
[15] S. Koh, P. Strasser, J. Am. Chem. Soc. 129 (2007) 12624–12625.
[16] J.X. Wang, H. Inada, L.J. Wu, et al., J. Am. Chem. Soc. 131 (2009) 17298–17302.
[17] S. Brimaud, R.J. Behm, J. Am. Chem. Soc. 135 (2013) 11716–11719.
[18] R. Loukrakpam, Q. Yuan, V. Petkov, et al., Phys. Chem. Chem. Phys. 16 (2014) 18866–18876.
[19] L. Peng, L. Gan, Y. Wei, et al., J. Phys. Chem. C 120 (2016) 28664–28671.
[20] S.E. Habas, H. Lee, V. Radmilovic, et al., Nat. Mater. 6 (2007) 692–697.
[21] D. Wang, Y. Li, Adv. Mater. 23 (2011) 1044–1060.
[22] D. Friebel, D.J. Miller, D. Nordlund, et al., Angew. Chem. Int. Ed. 50 (2011) 10190–10192.
[23] E. Christoffersen, P. Liu, A. Ruban, et al., J. Catal. 199 (2001) 123–131.
[24] S.H. Ahn, Y. Liu, T.P. Moffat, ACS Catal. 5 (2015) 2124–2136.
[25] W. Chen, R. Yu, L. Li, et al., Angew. Chem. Int. Ed. 49 (2010) 2917–2921.
[26] M.S.P. Jagannath, S. Divi, A. Chatterjee, J. Phys. Chem. C 122 (2018) 26214–26225.
[27] J. Suntivich, Z. Xu, C.E. Carlton, et al., J. Am. Chem. Soc. 135 (2013) 7985–7991.
[28] G. Tremiliosi-Filho, L.H. Dall'Antonia, G. Jerkiewicz, J. Electroanal. Chem. (Lausanne) 422 (1997) 149–159.
[29] Z. Yu, P.R. Cantwell, Q. Gao, et al., Science 358 (2017) 97–102.
[30] J.F. Nie, Y.M. Zhu, J.Z. Liu, X.Y. Fang, Science 340 (2013) 957–960.